aerospace

MDPI

Article

Design and Evaluation on Onboard Antenna Pointing Control System for a Wireless Relay System Using Fixed-Wing UAV

Koki Hamajima [1], Kei Yasukawa [1], Masazumi Ueba [1,*], Hisayoshi Kanou [2], Munehiro Matsui [2], Junichi Abe [2], Kiyohiko Itokawa [2] and Fumihiro Yamashita [2]

[1] Graduate School, Muroran Institute of Technology, Muroran 050-8585, Hokkaido, Japan
[2] NTT Access Service System Laboratories, NTT Corporation, Yokosuka 239-0847, Kanagawa, Japan
* Correspondence: ueba@mmm.muroran-it.ac.jp; Tel.: +81-143-46-5341

Abstract: Among several usages of unmanned aerial vehicles (UAV), wireless relay systems for high altitudes using fixed-wing UAVs, or high-altitude platform stations (HAPS), are some of the most promising applications. To realize the systems by making the most of advantages of the long flight duration and endurance of fixed-wing airplanes, this paper proposes an antenna pointing control system using mechanical gimbals onboard a fixed-wing UAV continuously turning midair and describes results of the blocking analysis of the antenna driving angles of the gimbal directed to a ground station, the design of the antenna pointing control system, and the evaluation of its performance. It is confirmed by the evaluation that, though the antenna pointing control accuracy is greatly influenced by the noisy antenna pointing direction command, its accuracy is greatly improved by using the highly accurate RF sensor to detect antenna pointing direction.

Keywords: HAPS; fixed-wing UAV; antenna pointing control system; wireless relay system; two-axis gimbal

Citation: Hamajima, K.; Yasukawa, K.; Ueba, M.; Kanou, H.; Matsui, M.; Abe, J.; Itokawa, K.; Yamashita, F. Design and Evaluation on Onboard Antenna Pointing Control System for a Wireless Relay System Using Fixed-Wing UAV. *Aerospace* **2023**, *10*, 323. https://doi.org/10.3390/aerospace10040323

Academic Editor: Mou Chen

Received: 31 October 2022
Revised: 21 February 2023
Accepted: 9 March 2023
Published: 23 March 2023

1. Introduction

Unmanned aerial vehicles (UAV), perhaps most notably represented by multicopters, have recently been used to provide diverse services, including the monitoring of crops and forests, measuring area, transporting commercial goods, relaying video and data, and inspecting tunnels, bridges, and buildings. Among the several uses of UAVs, wireless relay systems for high altitudes using fixed-wing UAVs [1,2], or high-altitude platform stations (HAPS) [3–7], are some of the most promising applications.

The concept of HAPS was formulated at the World Radiocommunication Conference in 1997, organized by the International Telecommunication Union (ITU) [3,7]. Since the 1990s, HAPS have been actively studied as radio relay stations using airships and airplanes that fly in the stratosphere where the airflow is relatively stable. Now that recent improvements in aircraft performance have reinvigorated the study of the technology, HAPS are drawing attention from telecommunication industries again and anticipated to support disaster-resistant and economical networks by performing wireless relay over a wide range, as shown in Figure 1. The fixed UAV flies and circles over the designated area in the stratosphere, with which communication equipment is equipped and the wireless communication link between mobile station and fixed station is established.

Generally speaking, fixed-wing UAVs have an advantage over multicopters in terms of long flight duration and endurance that makes them suitable for wireless relay that re-quires long-term flight. However, because fixed-wing UAVs cannot hover in the same po-sition, but have to constantly turn to stay midair, the antennas onboard UAVs have to be directed toward the designated ground station regardless of the turning motion of the UAVs.

There are many papers concerning payload pointing system [8–11]. Most of the systems are mounted on spacecraft, such as observation satellites [8–10] and space telescopes [11].

Therefore, the attitude motion of the spacecraft is very low, and its angular velocity is near zero. Besides, commands into the control system are almost constant, and all sensors onboard the spacecraft have a few noises compared to those of the UAV.

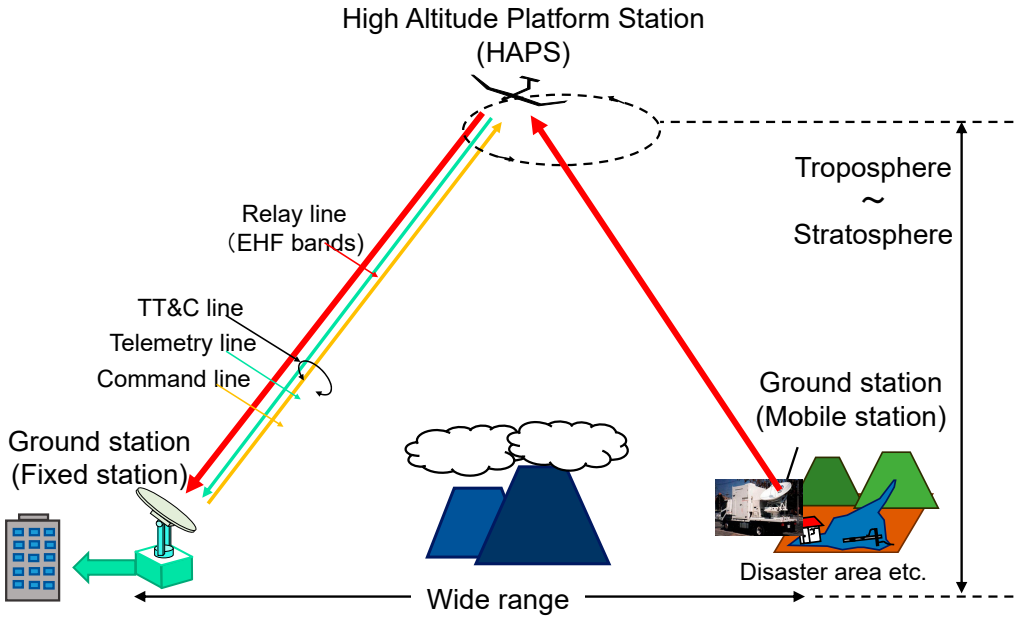

Figure 1. A HAPS-based wireless relay system.

In contrast, in case of the fixed wing UAVs, the UAVs are subject to a large disturbance represented by winds, and the disturbance causes large deviations of attitude angles and large attitude angular velocities of the UAV, and the body of the UAV may block the antenna direction. In addition, as the positions and attitudes of the UAV greatly change during its flight, the commands into the antenna pointing control system also greatly change every moment and should be generated by using measured attitude angles with relatively large noises.

In this situation, it is very important to clarify conditions both to avoid blocking the antenna direction by aircraft bodies and to realize highly accurate antenna pointing control systems for the designated ground station.

This paper is configured as follows. Section 2 describes the antenna pointing control system using mechanical gimbals. Next, Section 3 describes the blocking analysis of the antenna's pointing direction by a UAV during its turns in flight. Section 4 then explains how to determine an antenna's size and pointing accuracy, after which Section 5 de-scribes the configuration of the antenna pointing control system and its design method. Section 6 describes the results of simulations, and Section 7 concludes the paper and de-scribes future outlook on study.

2. The Antenna Pointing Control System

2.1. Mechanical Antenna Pointing Control

As shown in Figure 2, there are two methods of directing antennas: electronic scanning and mechanical scanning. The merits and demerits of both methods are summarized in Table 1. Whereas electronic scanning has been investigated for directing antennas in HAPS [12,13], mechanical scanning has usually been studied only in combination with electronic scanning [14,15]. In our study, by focusing on the gain fluctuation and pointing accuracy in relation to weight, we studied the antenna pointing control system based on mechanical scanning with a two-axis gimbal system [16].

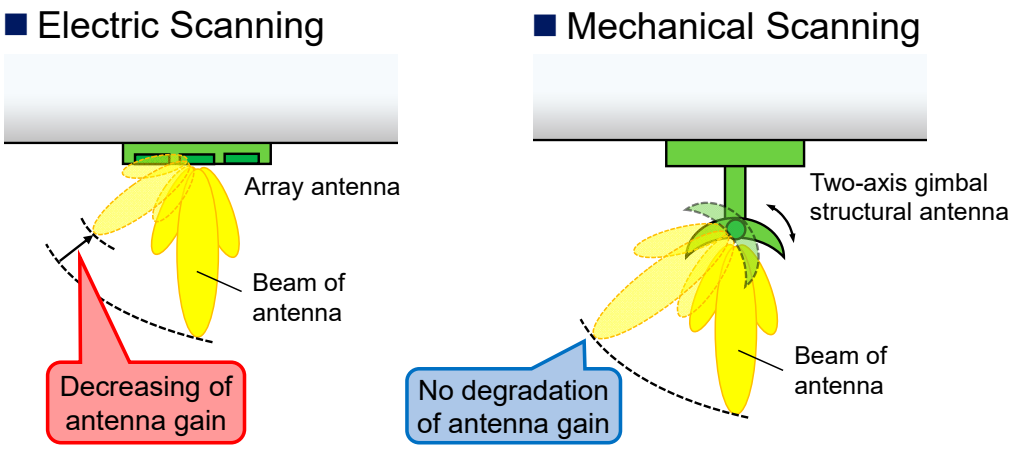

Figure 2. Antenna scanning method.

Table 1. Merits and demerits of two scanning method.

	Electrical Scanning	Mechanical Scanning
Gain fluctuation	Large	Small
Pointing accuracy	Inverse proportional to number of arrays	Constant
Weight	Inverse proportional to pointing accuracy	Constant
Complexity	Proportional to number of arrays	Constant

2.2. Proposed Antenna Pointing Control System

The proposed mechanical antenna pointing control system has mechanical two-axis gimbals mounted on board a fixed-wing UAV, as shown in Figure 3. To relay a wireless circuit, it is necessary to equip two antennas, each driven by a two-axis gimbal, on the fixed-wing UAV. In addition, these antennas are covered with a radome to reduce air re-sistance.

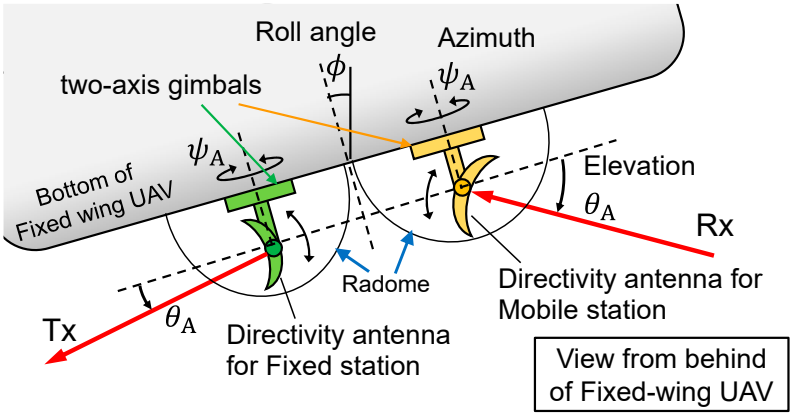

Figure 3. Antenna with two-axis gimbal onboard a UAV.

Realizing the proposed antenna pointing control system requires investigating the command antenna's driving angle, including conditions to block the antenna's direction by the UAV body itself, the required pointing accuracy, and motional interferences be-tween the UAV and the two-axis gimbal.

As the UAV turns, the direction of the onboard antenna should change, corresponding to the roll angle, heading angle, and the positions of the UAV. If the roll angle increases, depending on the distance between the UAV and the ground station, as well as on the altitude, then the UAV body may block the antenna's direction. Therefore, the antenna's direction angle with respect to body-fixed coordinates is analytically derived by using the

attitudes and positions of the UAV as parameters, which can clarify the conditions in which the antenna's direction is blocked by the UAV body.

The required pointing accuracy is critical for the antenna pointing control system. The required accuracy can be determined according to the antenna's size, i.e., antenna pattern, the frequency used, and transmitting power, so as to satisfy the ITU's Recommen-dations and Report [17,18].

Another problem peculiar to mechanical scanning antennas is that the drive of the antenna influences the motion of the UAV, thereby resulting in a change in the antenna's direction. Conversely, the motion of the UAV also influences the motion of the antenna—that is, the two-axis gimbal. Those effects can be clarified by analyzing the dynamics of the UAV attitude and the antenna driven by the two-axis gimbal.

3. Antenna Pointing Direction and Its Blockage by UAVs

3.1. Target Commands of Antenna Driving Angle

In the proposed system, two-axis gimbals with directional antennas are attached to the underside of the fixed-wing UAV to establish a wireless link between a fixed-wing UAV for relay and one ground station. The gimbals point the antenna's main beams toward the ground station by driving the azimuth and elevation angles. The target antenna's pointing direction is calculated by using the turning position and attitude of the fixed-wing UAV and the position of the ground station, as shown in Figures 4 and 5.

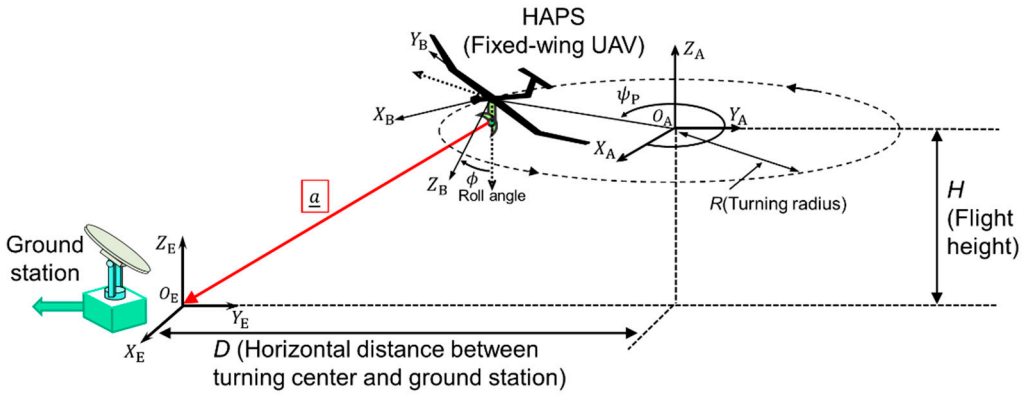

Figure 4. Position of the fixed-wing UAV and ground station.

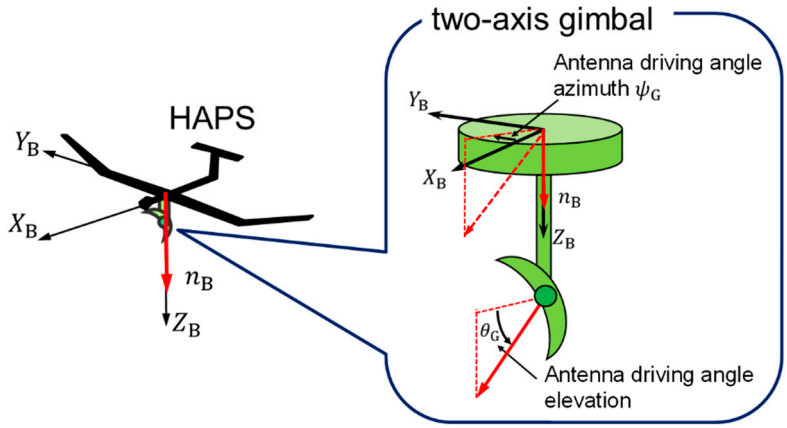

Figure 5. Driving angle of the two-axis gimbal.

In order to use the azimuth and elevation angles for the control system as target commands, those angles must be expressed in the body-fixed coordinates of the UAV. Those angles are calculated using the directional vector $\underline{a}$ from the UAV to the ground station, which is expressed in $X_E - Y_E - Z_E$ coordinates, as well as transforming it to $\underline{a_B}$, which is expressed in $X_B - Y_B - Z_B$ coordinates. Detailed operations are shown in Equation

(1)–(6) for the elevation angle target command θ_{GC} and in Equation (8)–(11) for the azimuth target command ψ_{GC}

The vector in the direction from the fixed-wing UAV to the ground station is expressed, as shown in Equation (1), by using positions for the UAV and the station expressed in $X_E - Y_E - Z_E$ coordinates. Position data for the UAV are measured by using the GNSS system.

$$\underline{a} = \underline{QO_E} = \begin{bmatrix} -R\cos\psi_P \\ -R\sin\psi_P - D \\ -H \end{bmatrix} \tag{1}$$

The transformation matrix between the ground-fixed coordinate system and the fixed-wing UAV's body frame coordinate system is defined as shown in Equation (2).

$$\begin{bmatrix} X_B \\ Y_B \\ Z_B \end{bmatrix} = \begin{bmatrix} \sin\psi_P & -\cos\psi_P & 0 \\ -\cos\psi_P\cos\phi & -\sin\psi_P\cos\phi & -\sin\phi \\ \cos\psi_P\sin\phi & \sin\psi_P\sin\phi & -\cos\phi \end{bmatrix} \begin{bmatrix} X_E \\ Y_E \\ Z_E \end{bmatrix} \tag{2}$$

Using the transformation matrix in Equation (2), the vector in Equation (1) is ex-pressed in the body frame coordinate system as in Equation (3).

$$\begin{aligned} \underline{a_B} &= \begin{bmatrix} \sin\psi_P & -\cos\psi_P & 0 \\ -\cos\psi_P\cos\phi & -\sin\psi_P\cos\phi & -\sin\phi \\ \cos\psi_P\sin\phi & \sin\psi_P\sin\phi & -\cos\phi \end{bmatrix} \underline{a} \\ &= \begin{bmatrix} D\cos\psi_P \\ H\sin\phi + (R + D\sin\psi_P)\cos\phi \\ H\cos\phi - (R + D\sin\psi_P)\sin\phi \end{bmatrix} \end{aligned} \tag{3}$$

By using the unit vector $\underline{n_B}$ in the Z-axis direction of the body frame coordinate system expressed in Equation (4), the inner product with $\underline{a_B}$ and $\underline{n_B}$ is calculated as shown in Equation (5).

$$\underline{n_B} = \begin{bmatrix} 0 \\ 0 \\ 1 \end{bmatrix} \tag{4}$$

$$\underline{a_B} \cdot \underline{n_B} = |\underline{a_B}|\cos\left(\frac{\pi}{2} - \theta_{GC}\right) \tag{5}$$

Defining parameters α and β, as shown in Equation (6), and by using the turning radius R, the horizontal distance D, and flight altitude H of the UAV, the elevation angle target command, θ_{GC}, is derived as shown in Equation (7).

$$\alpha = \frac{R}{H}, \beta = \frac{D}{H} \tag{6}$$

$$\theta_{GC} = \sin^{-1}\frac{\underline{a_B} \cdot \underline{n_B}}{|\underline{a_B}|} = \sin^{-1}\frac{\cos\phi + (\alpha + \beta\sin\psi_P)\sin\phi}{\sqrt{\alpha^2 + \beta^2 + 2\alpha\beta\sin\psi_P + 1}} \tag{7}$$

In the same way, in order to obtain the azimuth angle target command, the inner product between the directional vector $\underline{a_{B,xy}}$ shown in Equation (8), which is projected to $X_B - Y_B$ plane of the UAV, and the unit vector of the X-axis of the UAV, shown in Equation (9), is calculated as Equation (10).

$$\underline{a_{B,xy}} = \begin{bmatrix} D\cos\psi_P \\ H\sin\phi + (R + D\sin\psi_P)\cos\phi \\ 0 \end{bmatrix} \tag{8}$$

$$\underline{X_B} = \begin{bmatrix} 1 \\ 0 \\ 0 \end{bmatrix} \tag{9}$$

$$\underline{a_{B,xy}} \cdot \underline{X_B} = \left| \underline{a_{B,xy}} \right| \cos \psi_{GC} \tag{10}$$

In this case, the outer product between $\underline{X_B}$ and $\underline{a_{B,xy}}$ is used to judge the sign of the azimuth angle, as shown in Equation (11). The outer product vector, $\underline{X_B} \times \underline{a_{B,xy}}$, is shown in Equation (12).

$$\underline{X_B} \times \underline{a_{B,xy}} = \begin{bmatrix} 0 \\ 0 \\ Z_{op} \end{bmatrix} \tag{11}$$

$$Z_{op} = H \sin \phi + (R + D \sin \psi_P) \cos \phi \tag{12}$$

If the Z_{op} is bigger than or equal zero, the outer product vector will be upward, and the two-axis gimbal will be as shown in Figure 6. The azimuth target command, ψ_{GC}, is derived, as shown in Equation (13).

$$\psi_{GC} = \cos^{-1} \frac{\underline{a_{B,XY}} \cdot \underline{X_B}}{\left| \underline{a_{B,XY}} \right|} = \cos^{-1} \frac{-\beta \cos \psi_P}{\sqrt{(\beta \cos \psi_P)^2 + \{\sin \phi - (\alpha + \beta \sin \psi_P) \cos \phi\}^2}} \tag{13}$$

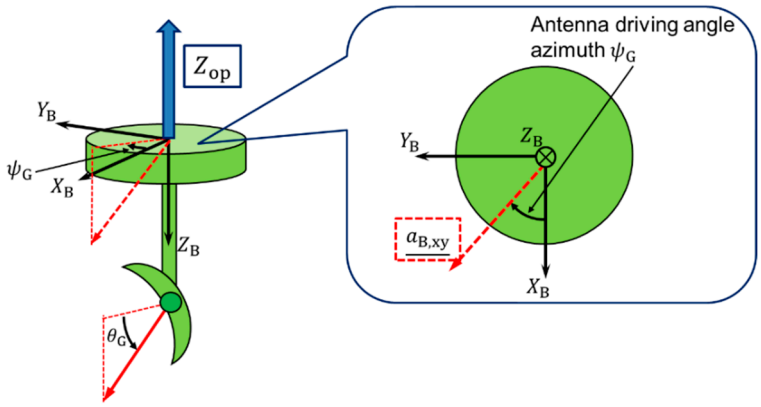

Figure 6. Two-axis gimbal when the Z_{op} is bigger than or equal to zero.

If the Z_{op} is smaller than zero, the outer product vector will be downward, and the two-axis gimbal will be as shown in Figure 7. Since the angle formed by the outer product is between 0° and 180°, the azimuth target command, ψ_{GC}, is derived, as in Equation (14), to represent an angle between 0° and 360°.

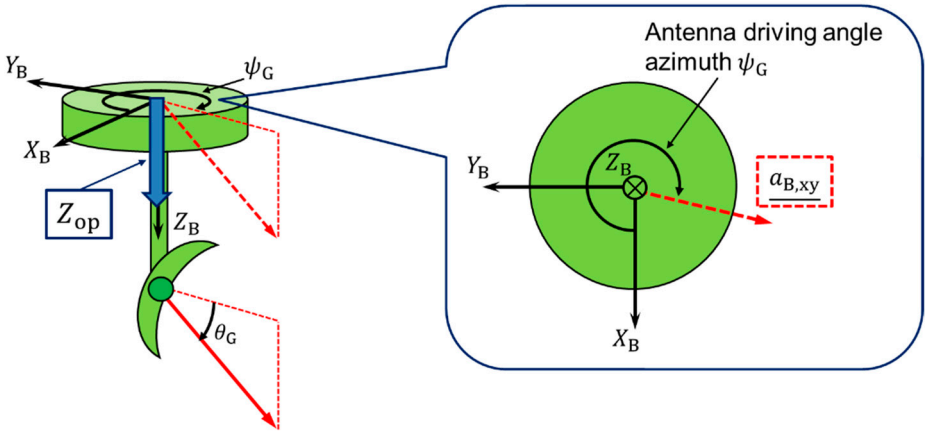

Figure 7. Two-axis gimbal when the Z_{op} is smaller than zero.

$$\begin{aligned}\psi_{GC} &= 2\pi - \cos^{-1}\frac{a_{B,XY}\cdot X_B}{\left|a_{B,XY}\right|} \\ &= 2\pi - \cos^{-1}\frac{-\beta\cos\psi_P}{\sqrt{(\beta\cos\psi_P)^2+\{\sin\phi-(\alpha+\beta\sin\psi_P)\cos\phi\}^2}}\end{aligned} \tag{14}$$

As a result of above operation, the elevation angle target command, θ_{GC}, is derived in Equation (7), whereas the azimuth target command is ψ_{GC}, which is derived in Equations (13) and (14). The θ_{GC} is the angle measured from $X_B - Y_B$ plane of the UAV, whereas the ψ_{GC} is the angle measured from the X_B-axis of the UAV.

3.2. Fluctuation of the Antenna's Drive Angle due to Turning

The fluctuations of the antenna's driving angles during turns in flight are calculated by using Equation (1). A result of antenna driving angle in elevation is shown in Figure 6, with $\alpha = 0.15$, $\beta = 7.5$, and ϕ as parameters. By defining the area blocked by the UAV as $\theta_{GC} < 0°$, the area can be determined, as marked in yellow in Figures 8 and 9. In short, as ϕ increases, is more likely to block the antenna's direction.

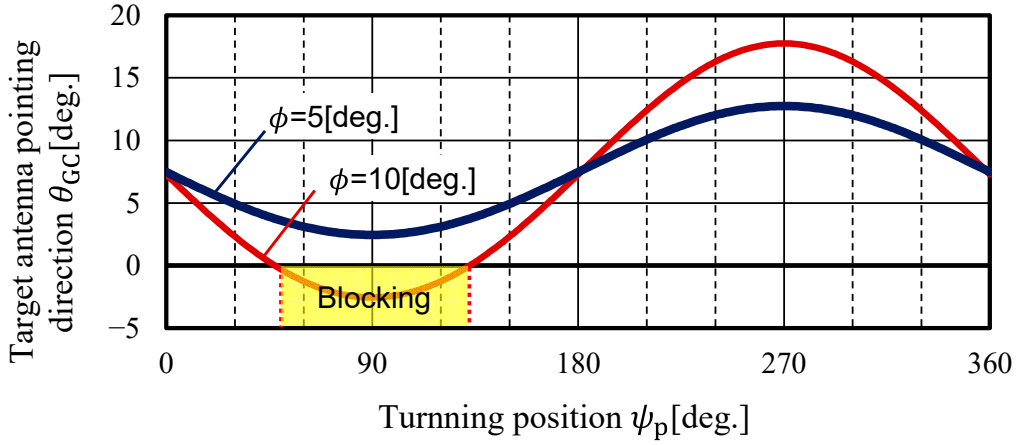

Figure 8. Fluctuation in gimbal elevation angle.

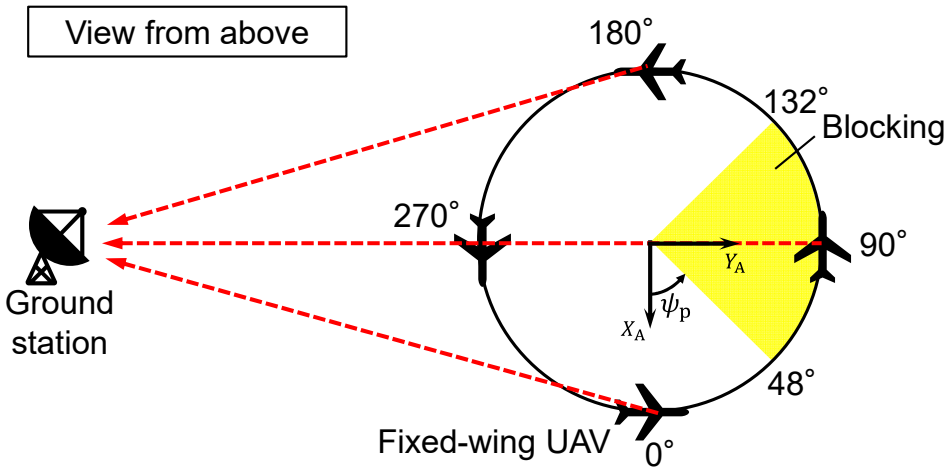

Figure 9. Fluctuation in gimbal elevation angle when $\phi = 10°$.

The fluctuation of the antenna's elevation angle when $\phi = 10°$ is expressed with respect to the heading and position of the UAV, as shown in Figure 9. As the UAV tilted left in the same direction as the target antenna, blocking occurred at $48° < \psi_P < 132°$.

3.3. Roll Angle to Avoid Blocking

Because the angles of the antennas are driven by two-axis gimbal changes, corresponding to the attitudes and positions of the UAV, it is important to know the conditions for avoiding blocking in advance. To return to Equation (7), when $\psi_P = 90$ degrees, θ_{GC} is as low as possible. Thus, if $\theta_{GC} < 0$ degrees when $\psi_P = 90$ degrees, blocking will inevitably occur. Conditions to avoid blocking can be clarified with Equation (1) by assigning $\theta_{GC} = 0$ degrees and $\psi_P = 90$ degrees, as shown Equation (15).

$$\phi < \tan^{-1} \frac{1}{\alpha + \beta} \tag{15}$$

Using Equation (4), the blocking area can be clarified in relation to β and ϕ. As examples of realistic values assumed in HAPS, the results in the case of α = 0.075 and α = 0.15 are shown in Figure 10a,b, respectively. Blocking can be prevented by flying HAPS under flight conditions that avoid the yellow blocking area in Figure 10. The results also confirm that the smaller that β and the velocity are, the bigger that α is and, in turn, the lower the risk of blocking.

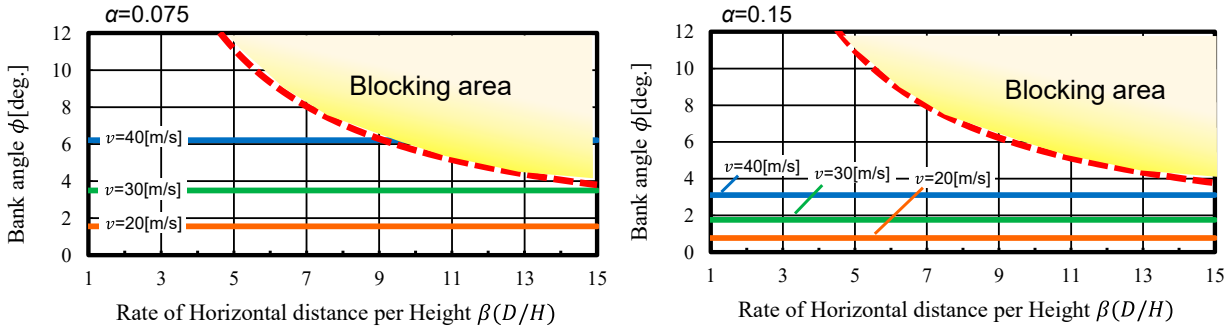

(**a**) (**b**)

Figure 10. Blocking area in relation to β and ϕ. (**a**) α = 0.075. (**b**) α = 0.15.

3.4. Blocking Judgement Flow

Figure 11 shows the flow to judge blocking of the antenna's pointing direction by UAV body. When blocking, change the communication method.

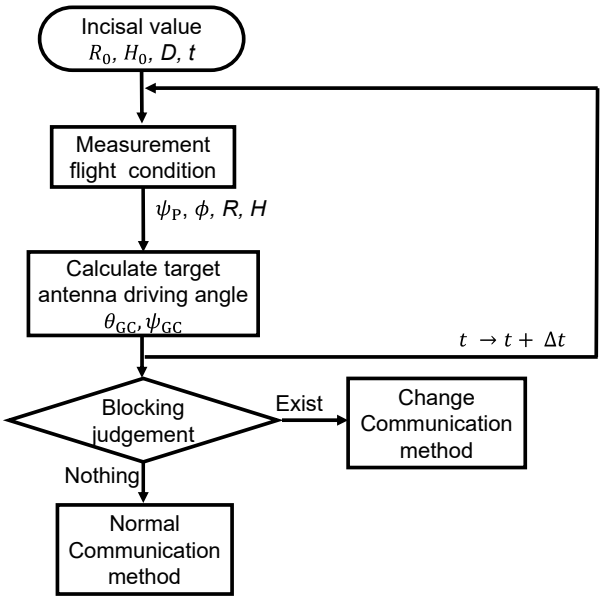

Figure 11. Blocking judgement flow.

4. Size and Target Pointing Accuracy of Antennas

The size of any antenna mounted on a fixed-wing UAV should comply with the ITU-R Recommendations and Report [17,18]. In particular, the maximum equivalent isotropically radiated power (EIRP) [17], taking into account the antenna pattern and transmitting power, should be lower than the specified values. At the same time, smaller antennas are desirable from the viewpoint of driving the inertia moment. Using recommendations applied to the extremely high frequency (EHF) [19] bands at 31.0–31.3 GHz, the antenna size can be calculated (Figure 12).

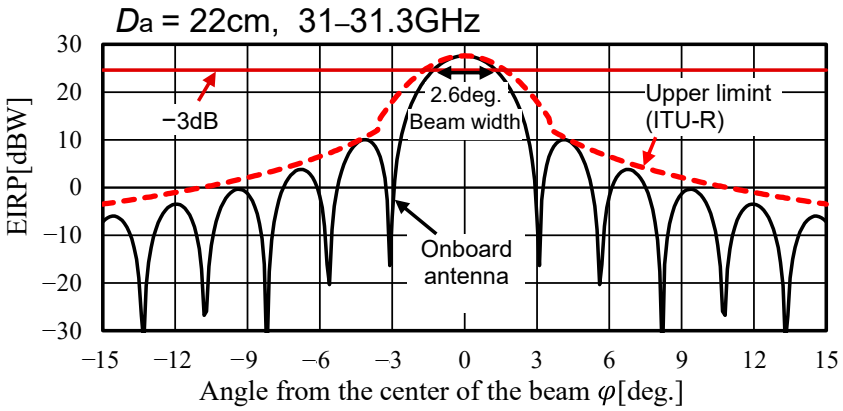

Figure 12. Antenna's EIRP compared with ITU-R Recommendations.

As a result, the size of D_a is 22 cm, and its beam's width is 2.6 degrees. If the antenna is smaller than 22 cm, then it will exceed the line specified by ITU Recommendations. By allowing less than 0.7 dB of deviation in the EIRP, the antenna's pointing accuracy was determined to be 0.13 degrees, or 1/20 of the beam's width.

5. Design of the Antenna Pointing Control System

5.1. Configuration

The configuration of the proposed antenna pointing control system, shown in Figure 13, consists of two independent control systems, an antenna driving control system, and a flight control system. Antenna pointing angles are measured by using a radio frequency sensor [20]. Generally, the two control systems interfere with each other as reaction torques. However, the magnitude of the interference depends on the magnitude of the inertia moment to be controlled in each system, which can be calculated by using the interference factor [21].

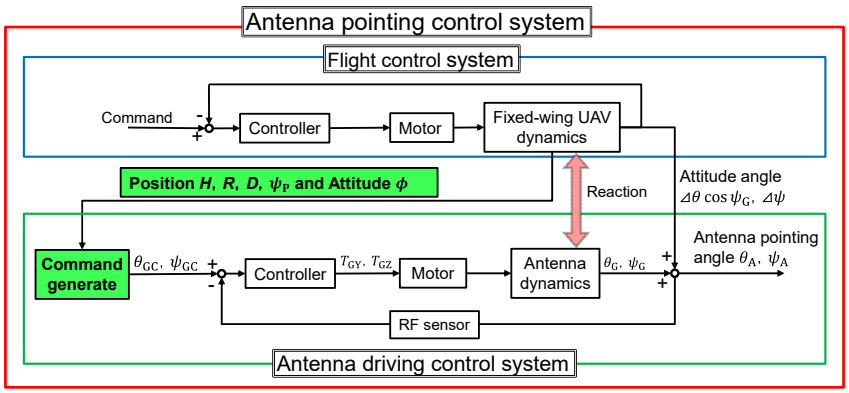

Figure 13. Antenna pointing control system.

Because the two-axis gimbal with the antenna is directly attached to the bottom of the fixed-wing UAV, the attitude angle error of the UAV is added to the pointing direction error.

As mentioned in Section 1, the commands into the antenna pointing control system change every moment and should be generated by using measured attitude angles. This means that commands themselves, shown in Equations (7), (13), and (14), should be calculated by using measured attitude angles ϕ and ψ_P, which may deteriorate antenna pointing accuracy. Therefore, it is very important to measure antenna pointing angles directly and accurately by using a RF sensor. The antenna driving control system controls the elevation angle and the azimuth angle independently, as shown in Figures 14 and 15 by using the commands.

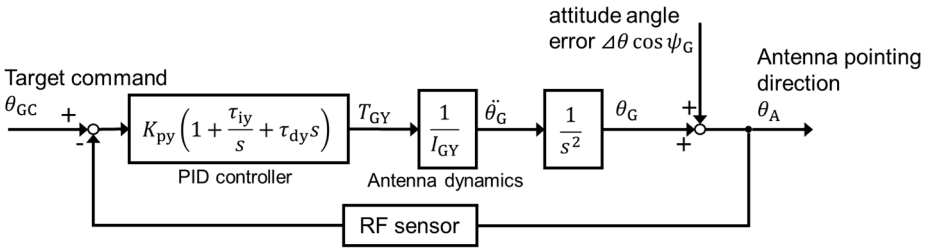

Figure 14. Antenna driving control system for elevation angle.

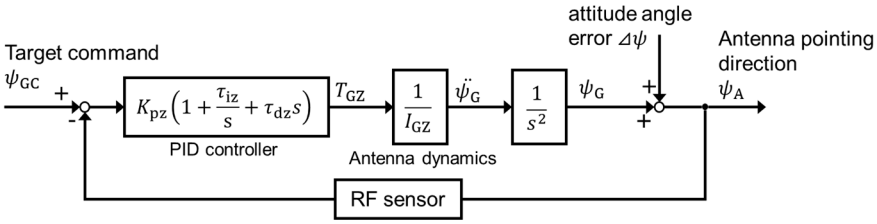

Figure 15. Antenna driving control system for azimuth angle.

5.2. Equation of Motion for the Fixed-Wing UAV and Two-Axis Gimbals

To design the proposed control system, it is necessary to clarify the rotational equation of motion for both the UAV and the two-axis gimbals. The reaction torques between the antenna driving control system and the flight control system are explicitly expressed in the equations and can be used to calculate the interference factor.

Equation (5) shows the rotational motion around each axis in the body-fixed coordinates of the UAV and the two-axis gimbals. The equation clarifies that the attitude angular acceleration of the two-axis gimbals multiplied by the inertia moment of the UAV works as a torque on the two-axis gimbals, while the drive of the angle angular acceleration of the two-axis gimbals multiplied by their inertia moment works as a torque on the UAV.

Because the two-axis gimbal structure for the antennas continues to rotate in the azimuth direction, the coordinate system does not match the aircraft axis of the fixed-wing UAV. As a result, the motion in the roll and pitch directions of the aircraft interferes with the driving of the elevation angle of the two-axis gimbals, and the motion in the yaw direction interferes with the driving of the azimuth angle.

$$\begin{bmatrix} I_{xx} & 0 & 0 & -I_{GY}\sin\psi_{AZ} & 0 \\ 0 & I_{yy} & 0 & I_{GY}\cos\psi_{AZ} & 0 \\ 0 & 0 & I_{zz} & 0 & I_{GZ} \\ -I_{GY}\sin\psi_{AZ} & I_{GY}\cos\psi_{AZ} & 0 & I_{GY} & 0 \\ 0 & 0 & I_{GZ} & 0 & I_{GZ} \end{bmatrix} \begin{bmatrix} \dot{p} \\ \dot{q} \\ \dot{r} \\ \ddot{\theta}_G \\ \ddot{\psi}_G \end{bmatrix} = \begin{bmatrix} L \\ M \\ N \\ T_{GY} \\ T_{GZ} \end{bmatrix}$$
$$+ \begin{bmatrix} I_{xz}\dot{r}+I_{xz}pq+(I_{zz}-I_{yy})qr+I_{GY}\left(r\dot{\theta}_G cos\psi_G+\dot{\theta}_G\dot{\psi}_G cos\psi_G\right)-I_{GZ}\dot{\psi}_G Q \\ -(I_{xx}-I_{zz})pr-I_{xz}(P^2-R^2)+I_{GY}\left(\dot{\theta}_G rsin\psi_G+\dot{\theta}_G\dot{\psi}_{AZ}sin\psi_G\right)+I_{GZ}p\dot{\psi}_G \\ I_{xz}\dot{p}-(I_{yy}-I_{xx})pq-I_{xz}qr-I_{GY}\left(p\dot{\theta}_G cos\psi_G+q\dot{\theta}_G sin\psi_G\right) \\ 0 \\ 0 \end{bmatrix} \quad (16)$$

5.3. Design

First, the interference between the two control systems can be calculated by the interference factor [21]. After the interference is found to be small enough for the gain margin and phase margin of classical control theory, the two control systems can be designed independently. The interference factor is obtained by converting the block diagram, as shown in Figure 16, for an example, into the form of a block diagram shown in Figure 17 and by calculating Equation (24). For simplicity's sake and for a worst-case scenario, equations of motion in Equations (17)–(19) are used, and the converted block elements are expressed in Equations (18)–(21).

$$I_{zz}\ddot{\psi} = T_Z - I_{GZ}\ddot{\psi}_G \tag{17}$$

$$I_{GZ}\ddot{\psi}_G = T_{GZ} - I_{GZ}\ddot{\psi} \tag{18}$$

$$\psi_A = K_B\psi_G + \psi \tag{19}$$

$$H_{11} = \frac{1}{I_{zz} - I_{GZ}} \cdot \frac{1}{s^2} \tag{20}$$

$$H_{12} = -\frac{1}{I_{zz} - I_{GZ}} \cdot \frac{1}{s^2} \tag{21}$$

$$H_{21} = \frac{1 - K_B}{I_{zz} - I_{GZ}} \cdot \frac{1}{s^2} \tag{22}$$

$$H_{22} = \frac{1}{I_{GZ}} \cdot \frac{K_B - (I_{GZ}/I_{zz})}{1 - (I_{GZ}/I_{zz})} \cdot \frac{1}{s^2} \tag{23}$$

$$\lambda = \sqrt{\frac{H_{12}H_{21}}{H_{11}H_{22}}} = \sqrt{\left|\frac{1 - K_B}{K_B - (I_{GZ}/I_{zz})}\right|} \tag{24}$$

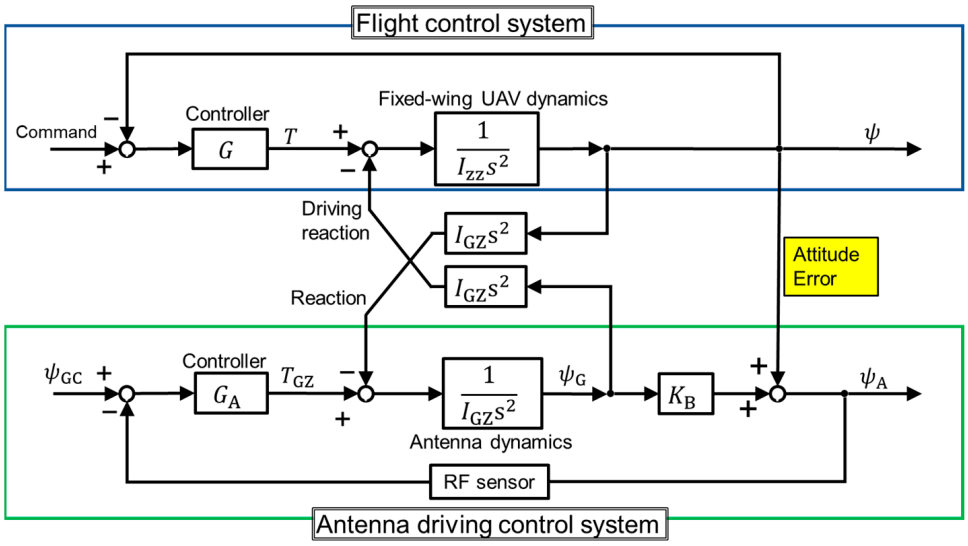

Figure 16. Block diagram.

In the control system, the ratio, K_B, of the fluctuation angle of the antenna's beam to the drive angle of the two-axis gimbal is 1, meaning that interference factor λ is 0. The same result was obtained for the elevation angle of the two-axis gimbal. Those outcomes show that the effect of interference between the two control systems is nil.

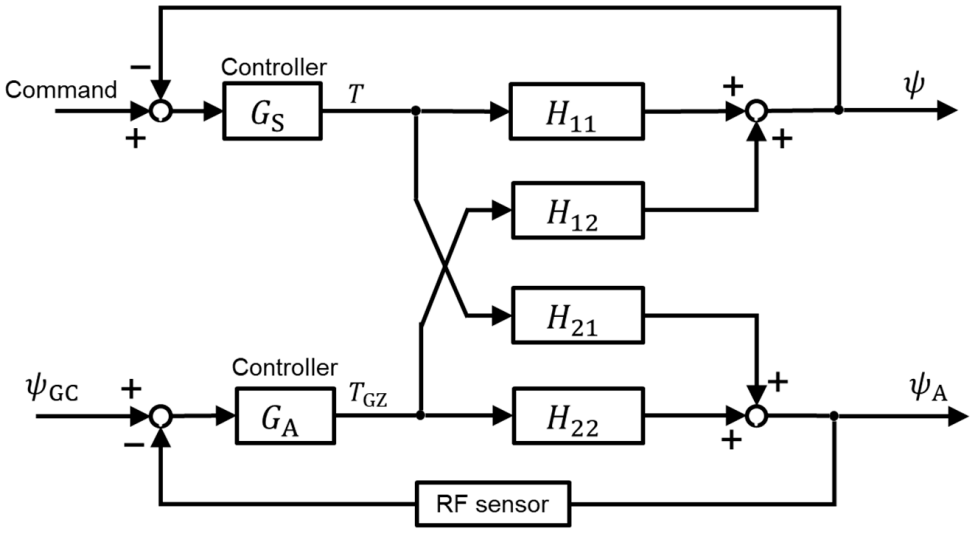

Figure 17. Format after conversion.

5.4. Control Frequency of Antenna Driving Control System

The control frequency required for antenna driving control system can be calculated from the required antenna pointing accuracy and the attitude angular velocity of the fixed-wing UAV, as shown in Equation (25) [22]. Therefore, the calculation results are shown in Figure 18.

$$\theta_{am} \geq \frac{\omega_{UAV}}{2\pi f_A} \tag{25}$$

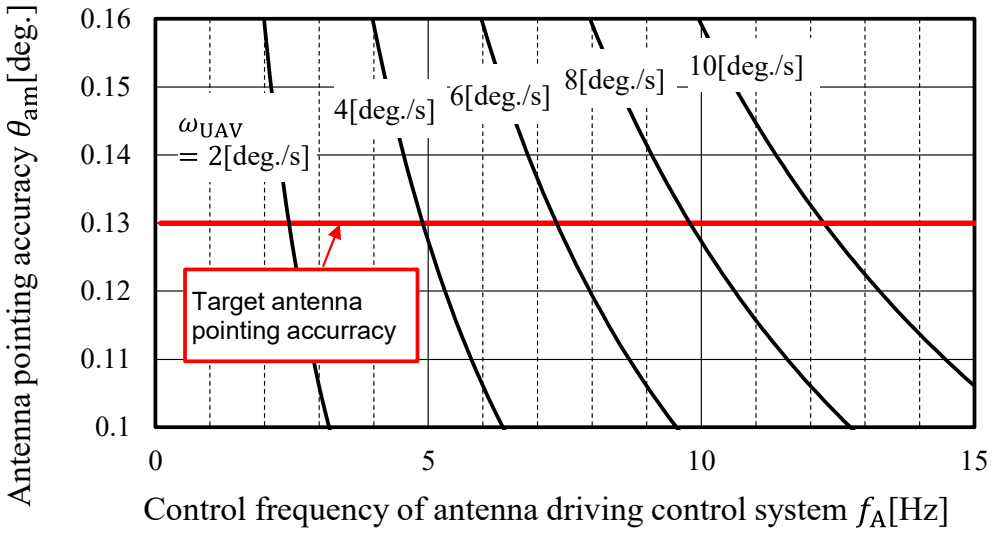

Figure 18. Control frequency of antenna driving against antenna pointing accuracy.

The average absolute values of the attitude angular velocities of the fixed-wing UAV are 4 deg./s for roll angular velocity, 7 deg./s for pitch angular velocity, and 4 deg./s for yaw angular velocity.

Therefore, the control frequency of the antenna driving control system was set to 10 Hz to be satisfied these.

6. Evaluation of Antenna Pointing Control Error

6.1. Conditions

A simulation of the antenna pointing control system was performed by using MATLAB and Simulink. Table 2 shows the parameters for the UAV and the onboard antenna.

Assuming that the UAV weighs 30–100 kg, we have adopted the UAV with a mass of 65 kg as an example.

Table 2. Parameters of the fixed-wing UAV and antenna.

I_{xx}	$[\mathrm{kg \cdot m^2}]$	37.4
I_{yy}	$[\mathrm{kg \cdot m^2}]$	25.2
I_{zz}	$[\mathrm{kg \cdot m^2}]$	55.7
I_{xz}	$[\mathrm{kg \cdot m^2}]$	0.033
I_{GY}	$[\mathrm{kg \cdot m^2}]$	0.01
I_{GZ}	$[\mathrm{kg \cdot m^2}]$	0.01

Table 3 shows the flight conditions and the positional relation between the UAV and the ground station as conditions of the simulation. In addition, the wind disturbance was set to 10 m/s with reference to the wind speed in the stratosphere [3].

Table 3. Conditions of the simulation.

α	-	0.15
β	-	7.5
v_0	[m/s]	30
W_d	[m/s]	10

Errors of attitude angles and accuracy of RF sensor are expected to greatly deteriorate antenna pointing accuracy. So, the pointing accuracy is evaluated by computer simulation assuming that all sensors except RF sensor are normal. The standard deviations of RF sensor are selected as a parameter.

Noises of sensors were considered to be random variables with a zero mean and a specified variance σ^2. The standard deviations σ for sensors used are summarized in Table 4. As for the RF sensor, its standard deviations are selected as 0.1, 0.05, and 0.01 degrees because the noise deviation should be less than the required antenna pointing accuracy of 0.13 degrees, mentioned in Section 4.

Table 4. Standard deviations of the noises of sensors.

Attitude (ϕ, θ, ψ)	[deg.]	0.5
H	[m]	0.2
RF sensor	[deg.]	0.1, 0.05, 0.01
v	[m/s]	0.17
GPS position	[m]	1

In this simulation, the attitude angle sensor noises become the error of the target command of the antenna driving angle. Therefore, the sensor output of the attitude angle is passed through a low-pass filter with a time constant of 0.3 s and used for the target command Equations (7), (13), and (14).

6.2. Stability Analysis

The controller, which consists of PID elements, for the antenna driving control system was designed by using classical control theory. The bode diagram of the open loop transfer function is shown in Figure 19. From the diagram, the influence can be secured. The phase margin is secured to be about 90 degrees. The crossover frequency of 10 Hz is secured.

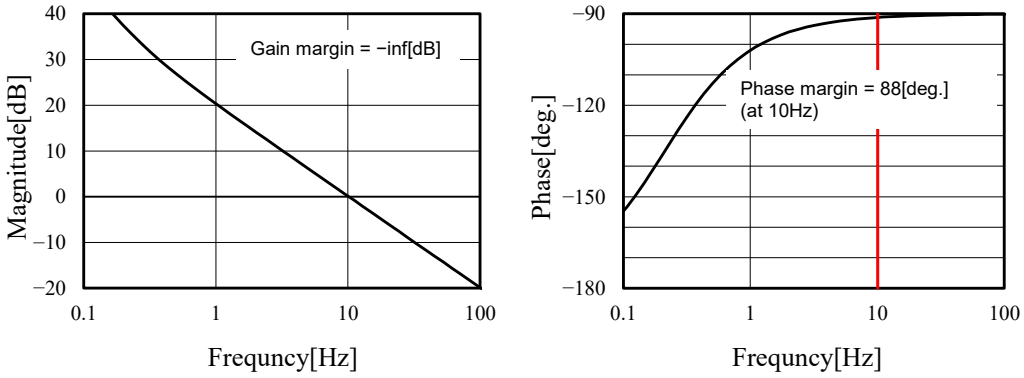

Figure 19. The bode diagram of antenna driving control system.

6.3. Results

Figures 20–25 show the results of the simulation in the listed conditions. Figure 20 shows the attitude angle profile of the UAV, Figure 21 shows the history of the target command of antenna driving angle, Figure 22 shows the history of the antenna's pointing directions, and Figures 23–25 shows the history of the antenna's pointing control errors. The antenna's pointing control error is the difference between the target antenna's drive angle and the antenna's pointing directions, as defined in Equations (15) and (16).

$$\Delta\theta_{\mathrm{A}} = \theta_{\mathrm{A}} - \theta_{\mathrm{GC}} \tag{26}$$

$$\Delta\psi_{\mathrm{A}} = \psi_{\mathrm{A}} - \psi_{\mathrm{GC}} \tag{27}$$

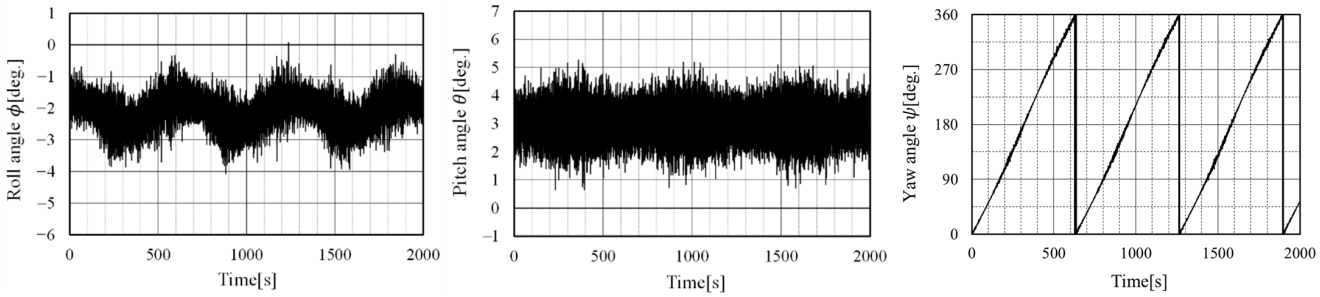

Figure 20. Time history of fixed-wing UAV's attitude. (**a**) Roll angle. (**b**) Pitch angle. (**c**) Yaw angle.

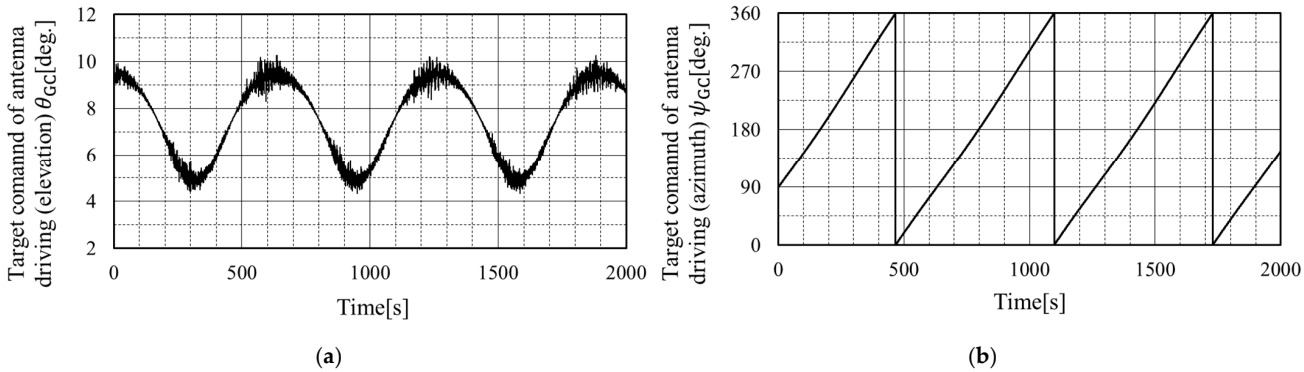

Figure 21. Time history of target command of antenna driving angle. (**a**) Elevation. (**b**) Azimuth.

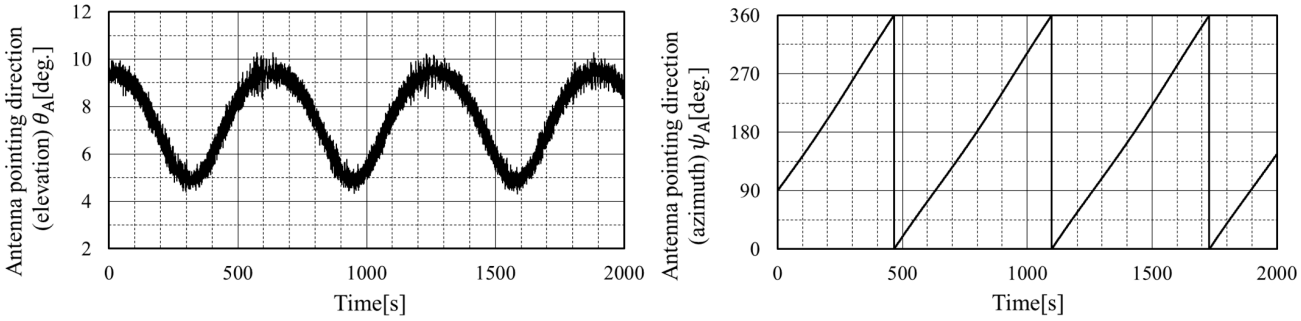

(**a**) (**b**)

Figure 22. Time history of the antenna's pointing directions. (**a**) Elevation. (**b**) Azimuth.

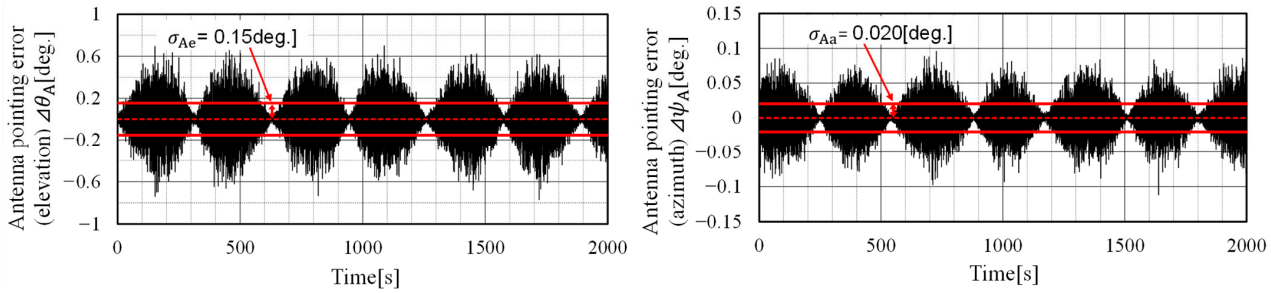

(**a**) (**b**)

Figure 23. Time history of the antenna's pointing control errors using RF sensor with 0.1 deg. accuracy directions. (**a**) Elevation. (**b**) Azimuth.

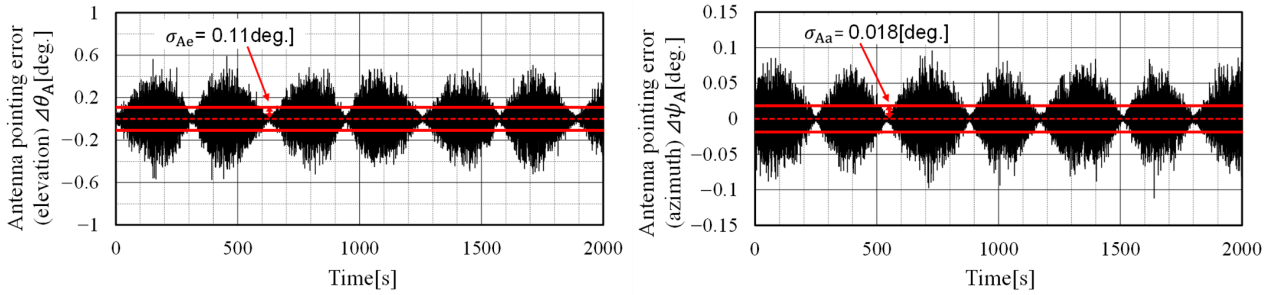

(**a**) (**b**)

Figure 24. Time history of the antenna's pointing control errors using RF sensor with 0.05 deg. accuracy directions. (**a**) Elevation. (**b**) Azimuth.

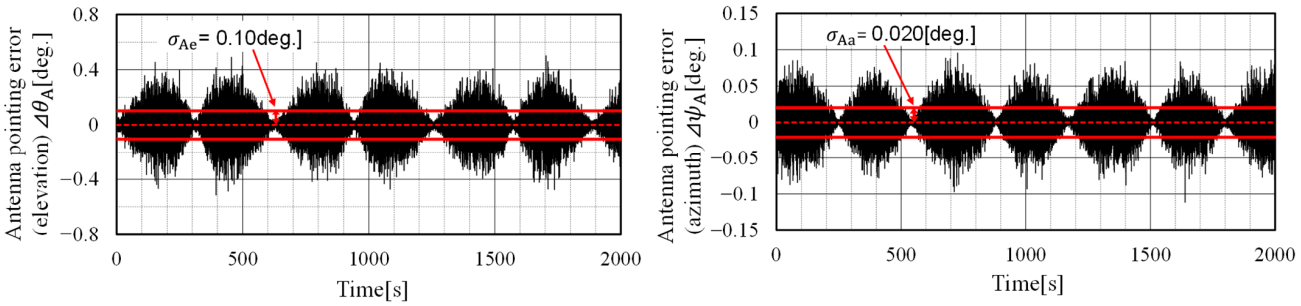

(**a**) (**b**)

Figure 25. Time history of the antenna's pointing control errors using RF sensor with 0.01 deg. accuracy directions. (**a**) Elevation. (**b**) Azimuth.

The results of the simulation confirmed that two control systems designed independently worked well. In the case of using commonly available sensors with standard deviations of 0.1 or 0.05 degrees for RF sensor, the target antenna pointing accuracy was not satisfied. However, when using a high-accuracy sensor of 0.01 degrees, regardless of attitude deviations, with a roll angle of ± 1.9 degrees, a pitch angle of 3.0 ± 2.4 degrees, and an azimuth angle of -0.8 ± 9.2 degrees, the antenna's pointing control errors as standard deviations were 0.10 degrees for the elevation angle and 0.020 degrees for the azimuth angle, respectively.

The results also confirmed that the design method is valid and the proposed antenna pointing control system meets the required antenna pointing control accuracy in terms of the standard deviation of the elevation and azimuth angle for typical fixed-wing UAVs for wireless relay stations. In addition, we found that the effect of noise from the RF sensor is important, given that the RF sensor requires a standard deviation of 0.01°.

7. Conclusions

We have proposed an antenna pointing control system to realize a wireless relay system using a fixed-wing UAV with two-axis gimbals able to stay in the stratosphere. We have also clarified the motion of the UAV's onboard antenna and the antenna pointing error via simulation, in addition to evaluating the antenna's pointing error. Given the results of the simulation, we have confirmed not only that the antenna pointing control system worked well, but also that the antenna pointing control error is greatly reduced and can achieve the required antenna pointing control accuracy using high accurate RF sensor with a standard deviation of 0.01 degrees and the validity of the control system's design. The antenna pointing control system for wireless relay UAV is characterized by time varying commands, which are generated by the noisy attitude angle and the highly accurate antenna pointing accuracy, which is deteriorated by the commands, and it is greatly improved by using a highly accurate RF sensor, which measures antenna pointing deviation from the target ground station. In further research, we will prepare hardware, such as fixed-wing UAVs and two-axis gimbals, and we will demonstrate results through flight experiments.

The HAPS will fly at an altitude of 20 km, with a temperature of -56 °C and an air density of 0.889 kg/m^3 [23]. The actual hardware to be developed must be within thermal operating range at that temperature and density. The antenna to be mounted on the aircraft will have a frequency of 31–31.3 GHz and a diameter of 22 cm, as defined in Chapter 4. For the demonstration experiment, the functionality of the antenna pointing control system will be verified first at low altitude.

Author Contributions: Methodology, M.U.; Software, K.Y.; Formal analysis, K.H.; Resources, H.K., M.M., J.A., K.I. and F.Y.; Writing—original draft, K.H.; Writing—review & editing, M.U., H.K., M.M., J.A. and K.I.; Project administration, M.U. and F.Y.; Funding acquisition, F.Y. All authors have read and agreed to the published version of the manuscript.

Funding: This research received no external funding.

Data Availability Statement: Data available on request due to restrictions e.g., privacy or ethical. The data presented in this study are available on request from the corresponding author. The data are not publicly available due to be used in future research.

Conflicts of Interest: The authors declare no conflict of interest.

Abbreviations

$\underline{a_{()}}$	vector of pointing	v_0	target turning flight velocity
$\underline{D}$	horizontal distance	W_d	wind disturbance
D_a	antenna diameter	$\underline{X_B}$	unit vector of UAV's X-axis
f_A	control frequency of antenna drive	$\overline{Z_{op}}$	Z element of $\underline{X_B} \times \underline{a_{B,xy}}$
H	flight altitude	α	ratio of radius and altitude
$H_{()()}$	the converted block elements	β	ratio of horizontal distance and altitude
$I_{()()}$	moment or product of inertia	θ	pitch angle of UAV attitude
K_B	ratio of fluctuation beam to drive	θ_{am}	antenna pointing accuracy
L	moment of X body axis	$\theta_{()}$	elevation angle
M	moment of Y body axis	$\Delta\theta_{()}$	control error of elevation
N	moment of Z body axis	λ	interference factor
$\underline{n_B}$	unit vector of UAV's Z-axis	σ	standard deviation of sensor noise
p	angular velocity of X axis	$\sigma_{A()}$	standard deviation of pointing error
q	angular velocity of Y axis	ϕ	roll angle of UAV attitude
r	angular velocity of Z axis	ψ	yaw angle of UAV attitude
R	turning radius	$\psi_{()}$	azimuth angle
$T_{G()}$	control torque of two-axis gimbal	$\Delta\psi_{()}$	control error of azimuth
v	turning flight velocity	ω_{UAV}	angular velocity of UAV

Subscripts

A	antenna pointing
B	in the body frame coordinate
G	gimbal driving
GC	target command of gimbal driving
x, y, z	body axis or gimbal axis
1, 2	block number

References

1. Derek, K.; Randal, B.; Timothy, M.; Michael, L.; Wei, R. Autonomous Vehicle Technologies for Small Fixed-Wing UAVs. In Proceedings of the 2nd AIAA "Unmanned Unlimited" Systems, Technologies, and Operations, AIAA-2003-6559, San Diego, CA, USA, 15–18 September 2003.
2. Masazumi, U.; Takuya, U. Study on Autonomous Flight Control for Tracking Meander Trajectory for Observation of Farm Land by Fixed-Wing UAV and Flight Verification. In Proceedings of the 58th Aircraft Symposium, JSASS-2020-5022, Online, Japan, 25–27 November 2020. (In Japanese)
3. Piera, D.V.; Daniel, F.M.; Spada, R.R. HAPS Operations and Service Provision in Critical Scenarios. In Proceedings of the SpaceOps Conference, Marseille, France, 28 May–1 June 2018.
4. Yunchou, X.; Frank, H.; Amitava, G.; Theodore, S.R. High Altitude Platform Stations (HAPS): Architecture and System Performance. In Proceedings of the 2021 IEEE 93rd Vehicular Technology Conference (VTC2021-Spring), Helsinki, Finland, 25–28 April 2021; pp. 1–6.
5. Atsushi, N.; Kenji, H.; Yoshichica, O.; Hideki, O.; Hideki, H. HAPS Radio Repeater System Using the Same System as Terrestrial Mobile Communications System. In Proceedings of the 2018 IEICE Society Conference, B-5-37, Ishikawa, Japan, 11–14 September 2018. (In Japanese)
6. Yohei, S.; Noboru, K.; Mitsukuni, K.; Kenji, H.; Yoshichika, O.; Atsushi, N. System Design of Gigabit HAPS Mobile Communication. *IEEE Access* **2020**, *8*, 157995–158007.
7. Ryu, M.; Masayuki, O. R&D Program on Telecom and Broadcasting System Using High Altitude Platform Station. *NICT* **2001**, *47*, 4.
8. Loh, Y.P. On antenna pointing control for communications satellite. In Proceedings of the 14th International Communication Satellite Systems Conference and Exhibit, AIAA-92-1940-CP, Washington, DC, USA, 22–26 March 1992.
9. Robert, O.H.; John, M.L. Pointing performance of a Space Station Freedom Payload Pointing System. In Proceedings of the Guidance, Navigation and Control Conference, AIAA-90-3351-CP, Portland, OR, USA, 20–22 August 1990.
10. Takanori, I.; Takeo, T.; Tetsuo, K.; Masakazu, A. Pointing Alignment Estimation for Precision Pointing Determination: Modeling, Estimation Method, and Calibration. In Proceedings of the AIAA Guidance, Navigation, and Control Conference, AIAA 2012-4784, Minneapolis, MN, USA, 13–16 August 2012.
11. Laskin, R.A.; Sirlin, S.W. Future payload isolation and pointing system technology. *J. Guid. Control Dyn.* **1986**, *9*, 469–477. [CrossRef]
12. Yohei, S.; Noboru, K.; Mitsukuni, K.; Kenji, H.; Yoshichika, O.; Atsushi, N. A System Design of Gigabit HAPS Mobile Communications with Energy Efficiency. *IEICE Tech. Rep.* **2019**, *119*, 359–364.

13. Shoichi, S.; Yohei, S.; Koji, T.; Wataru, T.; Kenji, H. Demonstration of Footprint Fixation and Area Optimization Using a Prototype Cylindrical Array Antenna for HAPS Service Link. *IEICE Tech. Rep.* **2021**, *121*, 29–34.
14. Morishige, H.; Hiroyuki, T.; Kouichi, M.; Moriyasu, M.; Yoji, A. Broadband Radio Communication System for Aircraft Using Millimeter-wave Band. *Mitsubishi Denki Giho* **2010**, *84*. (In Japanese)
15. Hiroyuki, T.; Ryu, M.; Takuya, O.; Tomoshige, K.; Takashi, M.; Morio, T.; Jun, S.; Yoshihisa, K. Development of 38GHz-Band Wireless Communication System Using High Altitude Platform Station (HAPS) for 5G Network: Examination of the 38 GHz-Band Ground Station Antenna for HAPS. In Proceedings of the 2021 IEICE General Conference, B-3-4, Online, 9–12 March 2021. (In Japanese)
16. Yuichi, T.; Yutaro, A.; Masazumi, U.; Shoichi, K.; Ken, H. Performance Evaluation Experiment of Highly Accurate and Responsive Tracking Antenna Control System for Simultaneous Observation by Unmanned Air Vehicles. In Proceedings of the IEICE Technical Report, SAT2016-66 (2017-02), Katsuura, Japan, 23–24 February 2017. (In Japanese).
17. International Telecommunication Union. *Report ITU-R F.2439-0*; Electronic Publication: Geneva, Switzerland, November 2018.
18. International Telecommunication Union. *Recommendation ITU-R F.699-8*; Electronic Publication: Geneva, Switzerland, January 2018.
19. International Telecommunication Union. *Recommendation ITU-R V.431-8*; Electronic Publication: Geneva, Switzerland, August 2015.
20. Broquet, J.; Claudinon, B.; Bousquet, A. Antenna pointing systems for large communications satellites. *J. Guid. Control Dyn.* **1985**, *8*, 71–77. [CrossRef]
21. Hiroshi, H. Effect of Antenna Drives on Attitude Control Systems. *Syst. Control Inf.* **1988**, *1*, 137–143. (In Japanese)
22. Yoichi, K.; Hiroshi, H.; Masazumi, U. Analysis of an Onboard Antenna Pointing Control System. *J. Guid. Control Dyn.* **1990**, *13*, 762–763.
23. Mikihiko, M.J. *Inst. Electr. Eng. Jpn.* **2002**, *12*, 525–527. (In Japanese)